

Aggregation and chimney formation during the solidification of ammonium chloride

T.H. Solomon*, R.R. Hartley† and A.T. Lee†

Department of Physics, Bucknell University, Lewisburg, PA 17837

(May 17, 1999)

Abstract

Experiments study large-scale pattern formation during the growth of ammonium chloride (NH_4Cl) from solution in a thin (Hele-Shaw) geometry. In particular, “mushy layers” form in which growing solid NH_4Cl crystals form a solid network interspersed with liquid. There are different ways that the mushy layer can be formed, however. If the cell is heated from below and cooled from above, thermal convection generates large-scale recirculating flows that carry seed crystals from the upper (cold) boundary to the (warmer) side and bottom boundaries. Ballistic deposition of these seed crystals leads to aggregation patterns with significant voids (filled with liquid) with a wide range of length scales. If the cell is cooled from below with a warm environment, the solid NH_4Cl grows dendritically without deposition, resulting in a compact mushy layer. Plume convection within this mushy layer produces one or two well-defined “chimneys.” If the environment is cool (comparable to the liquidus temperature of the solution), the mushy layer forms by a combination of dendritic growth and ballistic deposition, resulting in a more permeable mushy layer and enhanced chimney formation. The effects of ballistic deposition are enhanced if the cell is tipped, in which case the voids reappear. Plume convection and chimney formation are dramatically enhanced in this case. Additional experiments are done in which fluid flows in the system are

enhanced artificially to verify that enhancements in chimney formation are due primarily to the aggregation process, and not to the increases in fluid flows due to thermal and compositional convection.

81.30.Fb, 61.43.Hv, 68.70.+w, 47.20.Bp

I. INTRODUCTION

The solidification of a material from a melt or aqueous solution is a process that depends critically on the flows present in the system. Flows can arise for several reasons: (a) density variations coupled with gravitational forces can result in compositional or thermal convection [1]; (b) surface tension variations can produce Bénard-Marangoni convection [2]; (c) changes in the density of the material when solidified can drive flows even in the absence of gravity [3]; and (d) flows can be induced artificially as part of an industrial process. Because of the prevalence of flows in solidification processes, there is a great deal of practical interest in understanding the interplay between fluid flows and the solidification process.

Fluid flows affect both the basic morphological instabilities and the patterns that form in the solidification process. [4] For instance, shearing flows have been predicted [5] to enhance the stability of the faceted crystal growth. Fluid flows have also been demonstrated (both theoretically and experimentally) to influence the shape of growing dendrites. [6] On a larger scale, growing dendrites typically form a permeable solid-liquid “mushy layer” through which the fluid can flow. [7,8] These flows can dissolve the dendrites themselves, carving out channels (“chimneys”) into the growing solid. [9]

This paper focuses on another solidification mechanism that is also strongly dependent on fluid flows – aggregation. Although studied extensively in other systems [10–13], aggregation phenomena have received little attention in the solidification literature. Small seed crystals are carried by flows in the system, and deposited at the edges and bottoms of the apparatus, producing highly permeable structures. In typical, three-dimensional, terrestrial solidification experiments, these structures are not easily observed because they collapse under their own weight. However, aggregation structures could survive for microgravity-based fabrication processes. In addition to the patterns that form because of the aggregation process, the enhancements in permeability due to aggregation leads to significant enhancements in chimney formation as well.

The particular system studied here is the solidification of ammonium chloride (NH_4Cl)

from aqueous solution. This system has been studied extensively due to the similarities between the solidification process of NH_4Cl and that of metallic alloys. [7] Unlike their metallic counterparts, NH_4Cl solutions are transparent, permitting real-time investigation of the solidification process. The experiments presented here are conducted in a narrow geometry to preserve the aggregation structures before they collapse under their own weight. By manipulating the temperatures at the cell boundaries and by altering the orientation of the cell, we are able to produce different types of mushy layers and compare plume convection and chimney formation in the various situations.

In Section II, we discuss previous studies of aggregation and chimney formation. The experimental techniques are explained in Section III. The experimental results are presented in Section IV, along with some simple numerical simulations of the aggregation phenomena. The paper concludes with a summary and discussion section (Section V).

II. BACKGROUND

A. Mushy layers, compositional convection and chimney formation

For a growing crystal, the main order parameter is the propagation speed of the interface between the liquid and solid regions. If this speed is small enough, the interface remains flat and the resulting solid is a faceted crystal. For larger growth speeds, the interface undergoes an instability to the growth of needle crystals (“dendrites”). [14,15] In typical solidification processes, a forest of dendrites (along with their side-branches) propagate through the system, resulting in a network of dendrites and their side-branches, interspersed with unfrozen liquid. The resulting layer – referred to as a “mushy layer” – is a porous medium through which unsolidified liquid can flow. [7,8] An interesting feature of these mushy layers is the fact that flows in a mushy layer couple to the growth process. Fluid in up-flow regions tends to be depleted of solute; as a result, dendrites tend to dissolve in these regions. By contrast, dendrites grow more rapidly in down-flow regions, where the fluid has a larger

solute concentration.

If a metallic alloy or an aqueous solution is cooled from below, unstable density gradients form in the liquid due to the removal of solute from solution by the upwardly-growing solid. These density gradients result in compositional convection both in the liquid directly above the mushy layer and within the mushy layer itself. [9,16] Convection in the mushy layer organizes into broad down-flow regions and narrow upward plumes. The plumes carve out channels in the mushy layer referred to as chimneys.

There have been several studies of the properties of chimneys. Instabilities of mushy layer have been addressed theoretically by Worster [17], Amberg and Homsey [18] and by Emms and Fowler [19]. Experimental measurements characterizing the onset of plume convection and chimney formation have been done by Sample and Hanowel [20], Chen and Chen [21], Tait and Jaupart [22], Tait, Jahrling and Jaupart [23], and by Chen, Lu and Yang [24]. Recent experiments have measured the internal properties of the mushy layer itself; specifically, the permeability [25] and the temperature field [26] have been measured in detail, showing the growth of plume convection and its relation with chimney formation.

B. Aggregation phenomena

Aggregation phenomena can be categorized either as diffusion-limited aggregation (DLA) [27] or ballistic deposition. Diffusion-limited aggregation is a process by which small particles randomly diffuse in a system until they touch another solid object, in which case they stick to that object. As the DLA structure forms, chains of stuck particles screen out regions making it difficult for additional particles to penetrate into the “fjords” of the structure. The result is a branching pattern that is interspersed with voids with a wide range of length scales; in fact, these patterns have been shown to have fractal characteristics. [27]

Ballistic aggregation is similar to DLA, except that the particles follow linear trajectories before hitting and sticking to the developing aggregation cluster. This process is very important for the growth of thin films on a substrate by vapor deposition or sputtering. It

has been observed experimentally that these processes result in porous structures, frequently with fractal scaling properties. [28] As is the case with DLA, screening plays a significant role in the formation of ballistic aggregation patterns.

There have been several numerical and theoretical studies of ballistic aggregation. [10–13] These studies found that if the particles strike the surface at an oblique angle, columnar structures grow with voids between the columns. The voids in the structure have been shown to have fractal scaling properties, in agreement with the previous experiments. There is a preferred orientation for these voids, although there is no universal relation between this preferred void orientation and the deposition angle (the void angle depends on the properties of the system).

The experiments in this paper demonstrate that ballistic aggregation can significantly affect the pattern formation process in solidification problems. As will be shown, depending on the flows and temperatures in the system, patterns can form that are very similar to those seen in the vapor deposition and sputtering systems. In addition, the aggregation process can result in significant enhancements in the permeability of the growing mushy layer, resulting in substantially increased chimney formation. These experimental results are supplemented with simple numerical simulations that illustrate the same phenomena.

III. EXPERIMENTAL TECHNIQUES

The solution used in these experiments consists of 26.5% NH_4Cl by weight in water, with a liquidus temperature of $17^\circ C$. (See Ref. [21] for a detailed plot of the phase diagram for NH_4Cl solutions.) The solution is contained in a narrow inner cell with height 8.0 cm, width 16.0 cm, and a gap thickness of 0.10 or 0.20 cm (Fig. 1). (All of the experiments presented are conducted in a 0.20 cm cell, unless otherwise noted.) The narrow gap thickness is chosen for two reasons: (1) the confining geometry prevents the aggregation structures from collapsing under their own weight; and (2) the quasi-two-dimensional configuration greatly simplifies the imaging of growing solid.

The side bounding walls of the inner cell are made from optically clear Plexiglas, and the other two boundaries are made out of copper which has been sprayed with a thin layer of varnish to inhibit chemical reactions. The gap thickness is set with thin Plexiglas spacers, and the entire inner cell is glued together with silicone glue/sealant. Temperatures at the boundaries are controlled independently at the two copper plates and at the plexiglass side-walls. The “hot” copper plate temperature is controlled with a film heater and a feedback controller. The “cold” copper bounding plate is attached to a Plexiglas cooling box through which a water/ethylene glycol mixture is pumped. The temperature of this cooling fluid is regulated with a Neslab temperature control bath. The inner cell is surrounded by an outer temperature-controlled box which is regulated independently with a separate bath. The entire apparatus can be oriented at any angle relative to the horizontal, with the cooling boundary at the bottom, top, side or at an angle.

The temperature of the hot plate T_h is typically $20.0^\circ C$ (unless noted otherwise), which is above the liquidus temperature of $17^\circ C$, while the outer temperature T_o is typically 13.0 or $15.0^\circ C$. The cold plate temperature starts each runs at the same value as T_o , dropping to approximately $-10.0^\circ C$ within the first 5 minutes of the run.

One of the Plexiglas side walls forming the inner cell is painted with temperature-sensitive liquid crystal paints and a layer of black paint that provides a dark background for the imaging. (See Ref. [26] for a complete description of how these liquid crystal paints can be used for visualization of the temperature field.) The solidification patterns are characterized with the use of a monochrome CCD video camera, whose images are digitized on a PC. In the experiments, the entire apparatus is first brought to the temperature of the outer box, then the temperatures of the hot and cold boundaries are changed to their final values during an interval of approximately 5 minutes.

Convective fluid flows in the system are manipulated by changing the boundary temperatures and by altering the angular orientation of the apparatus. When cooled from below, the flows present are due almost entirely to compositional convection. When cooled from above, compositional density gradients are stabilizing; however, thermal gradients produce unstable

density variations that give rise to thermal convection. Other (intermediate) orientations are characterized by the presence of both compositional and thermal convection.

We have no direct measurements of the flow velocities in these experiments. The addition of neutrally-buoyant tracer particles to determine the velocities would interfere with the growth process, as would flow measurements with hot-film anemometry. The best that we can do is to follow the small seed crystals of NH_4Cl in the flow; however, the significant buoyancy difference between these particles and the suspending fluid make them unreliable as velocity indicators. For the larger seed crystals (approximately 0.5 mm), the buoyancy difference is enough to enable them to descend even in upflow regions.

By observing the smaller seed crystals, we estimate roughly that the flow velocities due to convection range up to a few mm/s flow in the fluid regions. Flow velocities in the mush are significantly smaller; they range up to a couple of mm/min, [25] almost two orders of magnitude weaker than those in the liquid regions.

IV. EXPERIMENTAL RESULTS

A. Cooling from below: Chimney formation

When the apparatus is oriented with the cold plate at the bottom (and a warmer outer temperature T_o), compositional density gradients produce convective flows in the mushy and liquid regions. Density gradients due to thermal expansion are stable, so there is no thermal convection. As has been documented in previous experiments, [21–25] this configuration lends itself toward the formation of mushy layers and chimneys.

In a typical experiment with the system cooled from below (Fig. 2, with $T_h = 20^\circ\text{C}$, $T_c = -10^\circ\text{C}$ and $T_o = 13^\circ\text{C}$), a mushy layer starts to form at the bottom almost immediately after cooling down the cold plate. Growth of this mushy layer is accompanied by small-wavelength salt-finger convection in the fluid region directly above the mush. After 10 - 20 minutes, the mush becomes thick enough to support convection, [21,22,24] and plumes

form within the mush, along with well-defined chimneys. In our experiments, there are typically 2 or 3 plumes initially, but the number of plumes drops as the mush thickness increases, resulting in usually only one clear chimney by the end of the run. [26] There are clear interactions between different plumes in the system (and their associated chimneys). Occasionally, oscillatory time dependence is observed between two plumes/chimneys for as many as 4 oscillation periods. [26]

The chimney formation process can be quantified by considering the “void fraction” – the fraction of the total area of the mush that is devoid of crystals. Experimentally, this is determined by dividing the area of the voids (after binarizing the image) by the area of the envelope for the mushy layer. [29] The results are shown in Fig. 3 (bottom, solid curve). The void fraction f starts out near zero before initiation of plume convection, then slowly increases as the mushy layer plumes carve out chimneys in the structure. The small dip in f at 50 minutes corresponds to the filling in of one of the chimneys, a coarsening process that is described in a previous paper. [26] After 100 minutes (a time longer than that shown in Fig. 3), f levels off at a value of approximately 0.08.

B. Heating from below: convection and aggregation

If the NH_4Cl solution is cooled from above, density variations due to compositional effects are stable, so there is no compositional convection and no chimney formation. However, density variations due to thermal gradients are unstable, and thermal convection ensues.

The strength of the thermal forcing in these runs can be quantified with the use of a quasi-two-dimensional Rayleigh number that takes into account the drag on the flow due to the narrow gap thickness. [30] The normalized Rayleigh number is defined as $r = \frac{g\alpha\Delta T d w^2}{48\pi^2\nu\kappa}$, where α , ν and κ are the coefficient of thermal expansion, the kinematic viscosity, and the thermal diffusivity of the fluid, respectively, g is the gravitational acceleration, ΔT is the temperature gradient $T_{bottom} - T_{top}$, $d = 8.0\text{ cm}$ is the height of the inner cell, and $w = 0.10$ or 0.20 cm is the gap thickness. With this definition, $r = 1$ corresponds to the onset of

convection. In the experiments presented in this paper with the cell is heated from below, $r \approx 15$ for the $w = 0.10$ cm cell, small enough such that the convective flow should remain laminar.

Fig. 4 (with $T_h = 16^\circ\text{C}$, $T_o = 22^\circ\text{C}$ and $T_c = -3^\circ\text{C}$) shows a sequence of images from a run where the cell is oriented with the hot plate at the bottom. Early in the run, two large convection rolls (vortices) form, with fluid rising in the center of the cell and falling at the outsides. Although not visible in the images in Fig. 4, this flow can be seen by observing small seed crystals as they are carried by the flow. The seeds form in the vicinity of the cold plate at the top, and are carried by the flow around and down the sides, where they are deposited in the aggregation patterns. Fig. 5 shows enlarged images of the developing aggregation patterns. Screening plays a significant role in these patterns, evidenced by the gaps that form. The gaps in the structure are noted by their orientation preference: they are oriented predominately at an angle of $49 \pm 5^\circ$ relative to the normal to the side wall.

The gaps in the aggregation structure can be understood by considering the deposition process. As has been shown in earlier studies [10–13], if seed particles rain down on a surface at an angle, the resulting aggregation pattern will develop gaps with a range of scales, but with an orientation that depends on the deposition angle. Fig. 6 shows some numerical simulations of this process. These results were obtained with a two-dimensional DLA-based algorithm where a simulated particle (seed crystal) follows a semi-random walk towards the left edge of a square lattice, weighted toward a particular angle. When the seed reaches a lattice point corresponding to the “wall” at the left edge of the system or to another occupied lattice site, it sticks irreversibly, and another seed is introduced into the system. The preferred angle is implemented very simply by having the particles drift to the left in the simulations, but tilting the bounding wall at an angle. When the simulation is complete, the image is tilted back to make the “wall” vertical. By choosing one particular drift angle, we are effectively simulating the growth of the aggregation cluster at a particular location along the wall, since it is reasonable to expect that the angle of incidence of the seeds would depend on height in the experiments.

These simulations differ from previous ones in that the seed particles are not monodisperse, but rather resemble the experiments whereby the size of each seed crystal depends upon when it nucleated and how far it travelled before sticking to the structure. These effects are simulated roughly by assigning each seed one of four sizes with radius $r = 0, 1, 2$ or 3 pixels ($r = 0$ is a dot, the rest are circles). The sizes are weighted by a Poisson distribution with an average radius of 0.4 pixels (resulting in a strong bias toward the smallest size). Once assigned a size, the seed is placed randomly at the right side of the lattice and its random walk is initiated. When all is said and done, however, the results of the simulations are found not to depend significantly on size distribution.

Figs. 6 a, b and c show the resulting pattern for deposition angles $\alpha = 0, 37,$ and 72 degrees, measured from the normal to the side wall. The gaps that form for $\alpha = 72$ degrees are oriented at approximately the same angle ($44 \pm 8^\circ$) as those from the experiments (Fig. 5) ($49 \pm 5^\circ$). In Fig. 6d, the structure from Fig. 6c has been manipulated digitally to represent approximately the partial filling in of the aggregation structure by the continued dendritic growth of the crystals after sticking. Specifically, the image is dilated [29] repeatedly, thickening the branches until the pattern resembles those from the experiment. (The pattern in Fig. 6d was dilated, then spatially-averaged using a 3×3 Gaussian filter to smooth the edges of the pattern. [31]) The similarities between Fig. 6d and Fig. 5 indicate that the seed particles strike the side walls at an angle of approximately 70 degrees relative to the normal in the actual experiment.

There is a fundamental change in the convective flow that is apparent in Figs. 4b and c. The growth of the aggregation patterns from the sides of the cell reduces the width of the central liquid region. When the aspect ratio of that central region drops to near 1 , the system can no longer support two convection rolls, and the counterclockwise roll is eliminated. In Figs. 4b and c, a new aggregation pattern is observed forming in the central region, forming at the downflow of the single (clockwise) convection roll in this region.

The void fraction f for this experimental run (upper, dashed curve in Fig. 3) starts off quite high (approximately 0.6) but drops off continually, levelling off at a plateau of

approximately 0.33. The decline in f is largely due to the fact that the seeds continue to grow dendritically after sticking, as can be seen in Figs. 5c and 5d. The dendrites continue growing into the voids until the NH_4Cl concentration in these regions drops below the saturation point.

C. Aggregation-enhanced chimney formation

Aggregation patterns can form even if the cell is cooled from below if the temperature T_o of the environment is low enough to allow seed crystals to survive in the middle portions of the cell. In this case, the flows that carry the seed crystals are caused by compositional density gradients, and the patterns that form reflect the nature of this compositional convection. An example of such a run is shown in Fig. 7 ($T_c = -10^\circ\text{C}$, $T_h = T_o = 5.5^\circ\text{C}$ initially, then raised to 10°). Shortly after the lower plate temperature is lowered, solidification is initiated at the bottom of the apparatus. Unstable density gradients produced by this solidification produces medium-scale convection patterns near the bottom of the fluid layer, with 12 - 14 convection rolls. These convective flows, in turn, sweep up seed crystals that form near the bottom and carry them upward in the up-flow regions of the flow. The seeds continue to grow, however, and they eventually become too heavy for the up-flows to carry. The result is a downward “snow” of dendrites in the up-flow regions of the convective flow (some of this snow can be seen over the right-most 3 aggregation piles in Fig. 7 a and b).

The aggregation piles the form from the NH_4Cl snow form a mushy layer with a permeability that is substantially greater than that for a normal mushy layer composed of a pure dendritic network. Because of the higher permeability, it is much easier for the mush to support plume convection. (The Rayleigh number Ra_m for convection in the mush depends linearly on the permeability, [8] so if the permeability is enhanced, then the critical Ra_m for the onset of convection can be achieved with smaller density gradients.) As a result, plumes develop in each of the aggregation mounds, resulting in the eventual formation of five clear chimneys in the system (as opposed to the typical case with only 1 or 2 in the long-term).

[32]

The void fraction f doesn't capture the full impact of the aggregation phenomena for this experimental run. Small-scale differences in permeability are not picked up by the technique that determines f , which specifically looks for identifiable regions with no crystals (over an area larger than the pixel resolution, which is approximately 0.12mm^2). Nevertheless, a plot of f for this run (middle, long-dashed curve in Fig. 3) is significantly different from that for the standard chimney formation case of Fig. 2 (lower, solid curve in Fig. 3). f starts off much larger than for the standard chimney formation case, due to the "snow" which results in aggregation and a porous mushy layer, similar to those seen in the simulations with deposition angle $\alpha = 0$ degrees (Fig. 6a, which should be viewed on its side to compare with Fig. 7). f continues to increase as the chimneys develop, then levels off and decreases slightly as the mush settles somewhat and some of the chimneys fill in slightly due to continued dendritic growth and coarsening.

If the apparatus is tipped at an angle, the convection takes the form of a single large recirculating flow encircling the entire inner cell. This "wind" blowing across the cold boundary carries seed crystals, so the mushy layer grows by a combination of dendritic growth and aggregation. If the tilt angle is small, the convective wind is weak, and the mushy layer is primarily dendritic. Furthermore, any seed crystals that form are deposited at a small deposition angle α , resulting in aggregation patterns with few voids, as seen in the simulations of Fig. 6a. On the other hand, if the tilt angle is large, the convective flow is large enough to cause appreciable aggregation. The permeability of the aggregation structures is particularly enhanced in this case by the fact that the lateral component of the flow (relative to the cold boundary) results in a larger deposition angle α , producing an aggregation pattern with significant voids. The result is a mushy layer with significantly larger permeability than would be the case for a standard dendritic mushy layer.

As a result of the increase in the mush permeability, experimental runs with the cell tipped are characterized by significant enhancements in plume convection and chimney formation, as shown in Fig. 8 for 30° and 52° tilt angles. The voids present in these images are

not merely aggregation gaps (as in Fig. 5); visualization of the temperature field in the fluid during these runs (using a thermochromic liquid crystal technique described in Ref. [26]) show vigorous plumes emanating from these channels. However, the voids are not aligned with the gravitational direction. Furthermore, the voids appear almost immediately as the mush is formed, so it is likely that the voids are initiated as aggregation gaps (due to screening of the seed particles), and then the emerging plume convection follows the aggregation voids and enlarges them into chimneys.

A plot of the void fraction f versus the tilt angle θ of the cell is shown in Fig. 9. The magnitude of f is very sensitive to the choice of threshold intensity when binarizing the images for the analysis. Furthermore, there are significant variations in f from run to run, due to the fact that the addition or subtraction of only one chimney significantly alters f . (This variability is the basis for the large error bars.) Consequently, only the trend in the data in Fig. 9 is relevant. It is nevertheless clear that tipping the cell can result in enhancements in chimney formation by approximately a factor of four beyond the normal cases (i.e., without aggregation), such as in Fig. 2.

D. Effects of enhanced fluid flows on chimney formation

It is important to distinguish the effects of aggregation on chimney formation from the effects of the enhanced convective flow itself. Additional experiments have been done to distinguish these effects. Specifically, experiments are done in which the flows are enhanced artificially without aggregation to see whether the flows enhance chimney formation.

1. Enhanced shearing flows

The effects of enhanced *shearing* flows in the liquid region are investigated with the use of a peristaltic pump. Holes are drilled into the left and right sides of the inner cell (as viewed in Fig. 1), angled downward toward the middle of the cell bottom. The two ends of a flexible hose are glued into these holes and the middle portion of the hose is threaded into

a peristaltic pump. When operating, the pump draws fluid from one side of the cell and pumps it back into the other side, blowing fluid down and across the mush-liquid interface. [33]

The flow rates used in these experiments range up to 1.3 times the total fluid volume of the cell per minute, resulting in flow velocities at the interface which are more than an order of magnitude larger than natural convective flow rates from the previous sections. In these experiments, the cell is cooled from below ($T_h = 20^\circ\text{C}$, $T_c = -10^\circ\text{C}$ and $T_o = 15^\circ\text{C}$), similar to the runs from section IV.A. The outer temperatures in these runs were sufficiently large to avoid any significant advection of seed crystals or aggregation phenomena.

Throughout the entire range of flow velocities used, no appreciable changes are observed in the void fractions (Fig. 10). These results indicate that simple enhancements in the shearing flows in the liquid layer have little effect on plume convection within the mush and on the formation of chimneys.

2. Enhanced mushy layer flows

Flows *within* the mushy layer are enhanced artificially with the use of a magnetohydrodynamic (MHD) technique (Fig. 11a). Nd-Fe-B permanent magnets are embedded into one of the Plexiglas side walls. An electrical current is sent through the NH_4Cl solution, and this current interacts with the magnetic field from the magnets to force a flow. (See Ref. [34] for more details of this technique.) In the configuration shown in Fig. 11a, the result is a forced flow that is upward in front of the “S” magnets and downward in front of the “N” magnets. There are also upflow regions to the left and right of the magnet array.

It is not possible to characterize the forced flow velocities within the mushy layer. Tests of the MHD technique in the liquid region before cooling the cold plate reveal forced flow velocities of approximately 1 cm/s, roughly an order of magnitude larger than typical convective flow velocities. Within the mushy layer, the enhanced (MHD) flows (for large currents) are also presumably roughly an order of magnitude stronger than the natural convective flows,

although both the natural and forced flows are significantly smaller in the mushy layer than in the fluid regions, since the mushy layer is a tightly-packed porous medium. We do not have any direct measurements of the flow velocities in the mush, however.

The effects of these forced flows on the mushy layer are evident in Fig. 11b (with temperatures $T_h = 20^\circ\text{C}$, $T_c = -10^\circ\text{C}$ and $T_o = 15^\circ\text{C}$, again similar to the runs from section IV.A without flow enhancements). The mush permeability is clearly larger in the upflow regions, due to the fact that upflows in a mushy layer tend to dissolve dendrites. Surprisingly, however, the artificial flows do not significantly enhance chimney formation, as is shown in Fig. 12. Even though the forced upflows within the mushy layer decrease porosity, the flows never focus into tight, well-defined chimneys.

Other MHD forcing configurations were used to induce artificial flows in the horizontal directions within the mushy layer, again without any significant enhancements in chimney formation. In fact, with uni-directional horizontal forcing within the mushy layer, chimney formation is actually slightly suppressed, i.e., the void fraction is reduced, although the reduction isn't significant compared to typical fluctuations in the void fraction between experimental runs. Additional experiments are in progress to assess the possibility that it may be possible to *inhibit* chimney formation with the use of internal flow enhancements.

V. SUMMARY

We have demonstrated that aggregation phenomena can play a significant role in the solidification of NH_4Cl from an aqueous solution. If the cell is cooled from above and heated from below, thermal convection generates flows that sweep small seed crystals from the top surface and deposits them in aggregation structures at the sides and bottom of the apparatus. If the apparatus is cooled from below, aggregation can be important if the environment is cool enough to maintain seed crystals in the central region. In this case, seed crystals are carried upward from the bottom due to compositional convection and “snow” back down after growing. The snow then produces an aggregation pattern with a

significantly larger permeability than that due to purely dendritic growth of NH_4Cl from the cold boundary. The increase in permeability due to the aggregation results in significant enhancements in plume convection and chimney formation. These effects are even more pronounced if the cell is tilted at an angle, in which case there is a lateral component to the motion of the seed crystals (relative to the boundary), and the resulting aggregation patterns develop voids due to screening effects.

Additional experiments have been done with artificially forced flows both in the liquid and mushy regions. These experiments find no significant enhancements in plume convection or chimney formation, indicating that increases in convective flows themselves are not responsible for the enhanced chimney formation observed in the experiments with the cell tipped.

It should be noted that aggregation phenomena in solidification processes are usually not too significant for three-dimensional terrestrial processes since the aggregation structures collapse under their own weight. However, the current experiments demonstrate that aggregation can be very important for solidification processes in confined (2-D) geometries. Furthermore, these effects should be very significant for solidification processes in reduced gravity environments, since fluid flows are still present in those environments (except for buoyancy-driven flows).

It is also quite striking that artificial flow enhancements themselves do *not* result in appreciable enhancement of chimney formation. Additional experiments are in progress to assess whether flow enhancements might actually *inhibit* chimney formation.

The research presented here was supported by a Cottrell College Science Award of Research Corporation (grant CC4002). We are also pleased to acknowledge the assistance of Dave Vayda in the construction of the apparatus, and useful discussions with C. F. Chen.

REFERENCES

* Electronic mail: tsolomon@bucknell.edu

† Electronic mail: atlee@bucknell.edu

‡ Current address: Department of Physics and Center for Nonlinear and Complex Studies (CNCS), Duke University, Durham, NC 27707; email address: hartley@phy.duke.edu

- [1] S. H. Davis, in *Handbook of Crystal Growth, Vol 1B*, 859-897, ed. D. T. J. Hurle (North-Holland, Amsterdam, 1993).
- [2] C. Normand and Y. Pomeau, *Rev. Mod. Phys.* **49**, 581 (1977).
- [3] A. O. P. Chiareli and M. G. Worster, *J. Fluid Mech.* **297**, 293 (1995).
- [4] S.R. Coriell, G.B. McFadden, R.F. Boisvert, and R.F. Sekerka, *J. Cryst. Growth* **69**, 15 (1984); S.A. Forth and A.A. Wheeler, *J. Fluid Mech.* **202**, 339 (1989); A.K. Hobbs and Ph. Metzener, *J. Cryst. Growth* **112**, 539 (1991).
- [5] T. P. Schulze and S. H. Davis, *J. Cryst. Growth* **149**, 253 (1995).
- [6] S. C. Huang and M. E. Glicksman, *Acta Met.* **29**, 701 (1981); R. Ananth and W. N. Gill, *J. Cryst. Growth* **91**, 587 (1988); D. Canright and S. H. Davis, *J. Cryst. Growth* **114**, 153 (1991).
- [7] H. E. Huppert, *J. Fluid Mech.* **212**, 209 (1990).
- [8] M. G. Worster, *J. Fluid Mech* **224**, 335 (1991).
- [9] M. G. Worster, *Ann. Rev. Fluid Mech.* **29**, 91 (1997).
- [10] J. Krug and P. Meakin, *Phys. Rev. A* **40**, 2064 (1989).
- [11] P. Meakin and J. Krug, *Phys. Rev. A* **46** 4654 (1992).
- [12] R. N. Tait, T. Smy and M. J. Brett, *Thin Solid Films* **226**, 196 (1993).

- [13] M. J. Brett, *J. Mat. Sci. Lett.* **8**, 415 (1989).
- [14] W. W. Mullins and R. F. Sekerka, *J. Appl. Phys.* **35**, 444 (1964).
- [15] S.R. Coriell and G.B. McFadden, in: *Handbook of Crystal Growth, Vol. 1B*, 785, ed. D.T.J. Hurle (North-Holland, Amsterdam, 1993).
- [16] R. J. McDonald and J. D. Hunt, *Metall. Trans.* **1**, 1787 (1970).
- [17] M. G. Worster, *J. Fluid Mech.* **237**, 649 (1992).
- [18] G. Amberg and G. M. Homsey, *J. Fluid Mech.* **252**, 79 (1993).
- [19] P. W. Emms and A. C. Fowler, *J. Fluid Mech.* **262**, 111 (1994).
- [20] A. K. Sample and A. Hellawell, *Metall. Trans. A* **15**, 2163 (1984).
- [21] C. F. Chen and F. Chen, *J. Fluid Mech.* **227**, 567 (1991).
- [22] S. Tait and C. Jaupart, *J. Geophys. Res.* **97**, 6735 (1992).
- [23] S. Tait, K. Jahrling and C. Jaupart, *Nature* **356**, 406 (1992).
- [24] F. Chen, J. W. Lu and T. L. Yang, *J. Fluid Mech.* **276**, 163 (1994).
- [25] C. F. Chen, *J. Fluid Mech.* **293**, 81 (1995).
- [26] T. H. Solomon and R. R. Hartley, *J. Fluid Mech.* **358**, 87 (1998).
- [27] T. A. Witten, Jr. and L. M. Sander, *Phys. Rev. Lett.* **47**, 1400 (1981); H. E. Stanley, “Fractals and multifractals : the interplay of physics and geometry”, in *Fractals and Disordered Systems*, ed. A. Bunde and S. Havlin (Springer-Verlag, New York, 1993).
- [28] G. Radnoczi, T. Vicsek, L. M. Sander and D. Grier, *Phys. Rev. A* **35**, 4012 (1987); J. Zhang, *Phys. Rev. B* **41**, 9614 (1990); D. Le Bellac, G. A. Niklasson and C. G. Granqvist, *Europhys. Lett.* **32**, 155 (1995).
- [29] The envelope area is determined digitally: the image is binarized then “dilated” several

times, a process in which the nearest neighbors of every “on” pixel are also turned on, resulting in growth and filling in of the binarized pattern. The dilation process is repeated until all the voids are filled in. The image is then “eroded” the same number of times. (Erosion is the inverse of dilation, where the outer-most pixels of the pattern are turned “off.”) The result is a pattern with the same overall shape as the original, but without the voids. The area of this envelope is then determined by counting the number of “on” pixels.

- [30] A. A. Predtechensky, W. D. McCormick, J. B. Swift, Z. Noszticzius, and H. L. Swinney, *Phys. Rev. Lett.* **72**, 218 (1994).
- [31] J. C. Russ, *The Image Processing Handbook, Second Edition* (CRC Press, Boca Raton, 1995).
- [32] The aggregation patterns that form are often less clean than the pattern shown in Fig. 7. If there are any impurities or imperfections on the top copper plate, for instance, seed crystals may form preferentially at those impurities and “snow” down unevenly, resulting in uneven piles and fewer chimneys.
- [33] Two hoses are used in the pump and are arranged to be out of phase with each other to minimize the pulsing effects usually encountered with a peristaltic pump. Also, the portion of the hose outside the cell is cooled to minimize warm-up of the fluid being pumped.
- [34] H. Willaime, O. Cardoso, and P. Tabeling, *Phys. Rev. E* **48**, 288 (1993); T. H. Solomon, S. Tomas, and J. L. Warner, *Phys. Rev. Lett.* **77**, 2682 (1996); T. H. Solomon, S. Tomas, and J. L. Warner, *Phys. Fluids* **10**, 342 (1998).

FIGURES

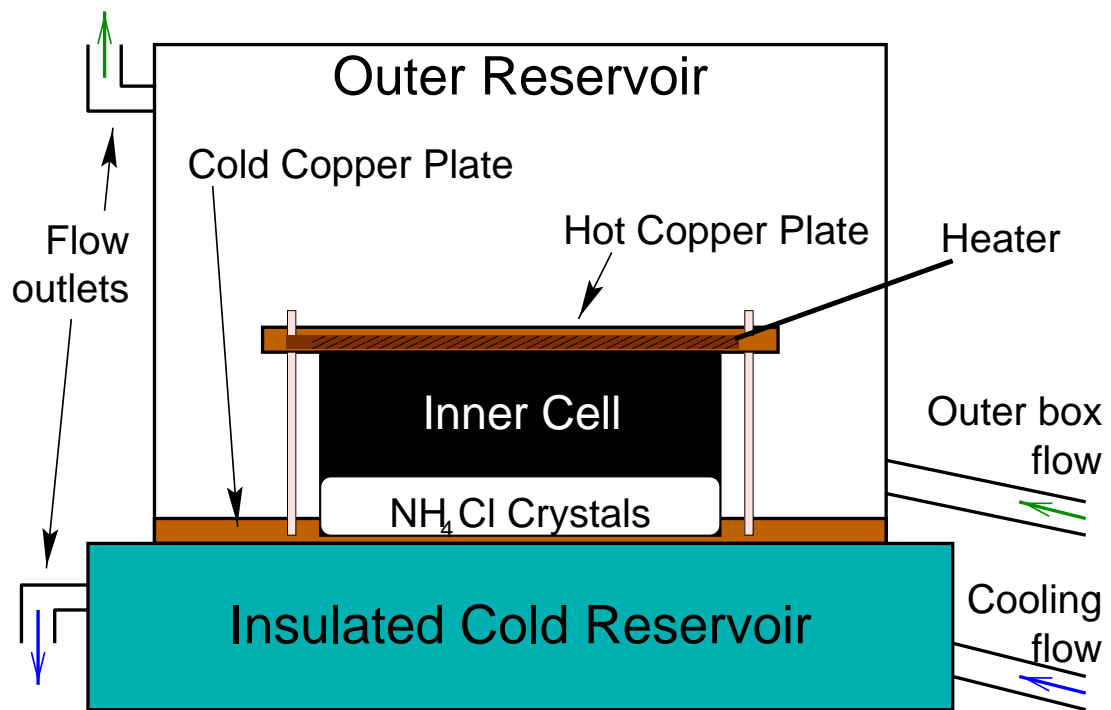


FIG. 1. Diagram of apparatus for the experiments. The inner cell is 8.0 cm high, 16.0 cm long, and has a thickness of either 0.10 or 0.20 cm.

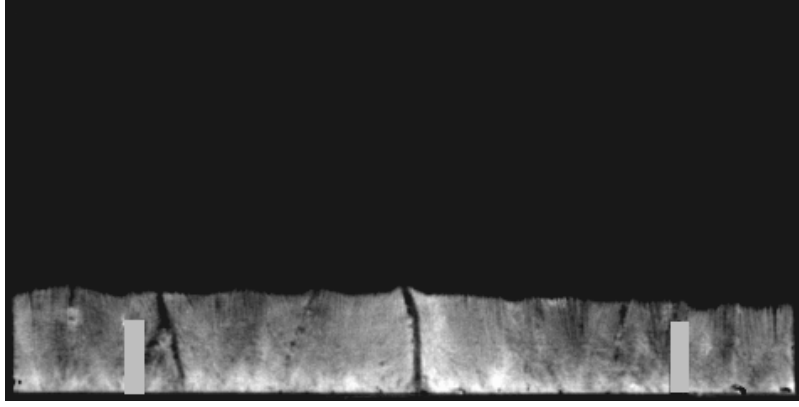


FIG. 2. Example of chimney formation when cooled from below; hot (upper) plate temperature $T_h = 20^\circ \text{C}$, cold (lower) plate temperature $T_c = -10^\circ \text{C}$, outer temperature $T_o = 13^\circ \text{C}$. The entire inner cell (8.0 cm x 16.0 cm) is visible. The gray rectangles at either side denote the locations of screws that block visualization of the mushy layer.

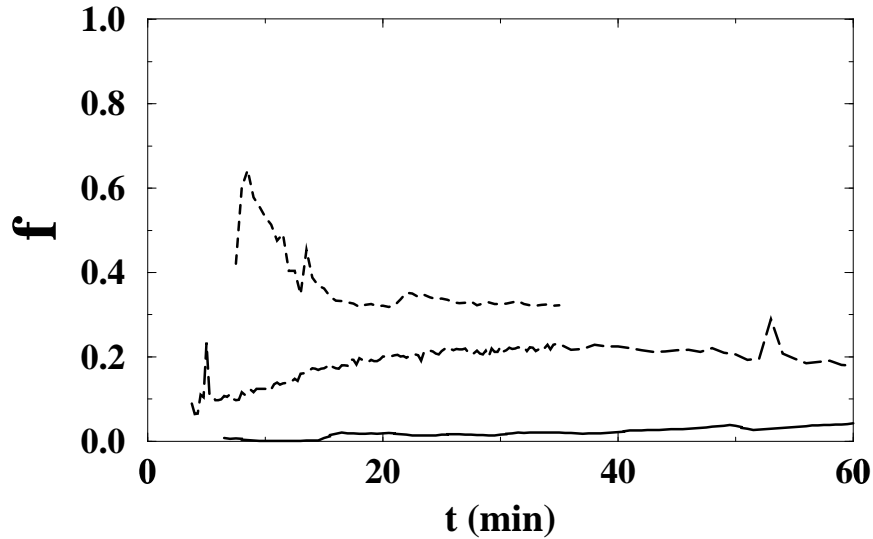


FIG. 3. Void fraction f : the fraction of area of the developing structure that is empty. Solid (lower) curve: data from Fig. 2, with the cell cooled from below and $T_o = 13^\circ \text{C}$ (standard chimney formation); dashed (upper) curve: data from Fig. 4, with the cell cooled from above and with $T_o = 22^\circ \text{C}$ (aggregation); long-dashed (middle) curve: data from Fig. 7, with the cell cooled from below but with a cool outer temperature ($T_o = 5.5^\circ$ initially, then raised to 10° after 10 min).

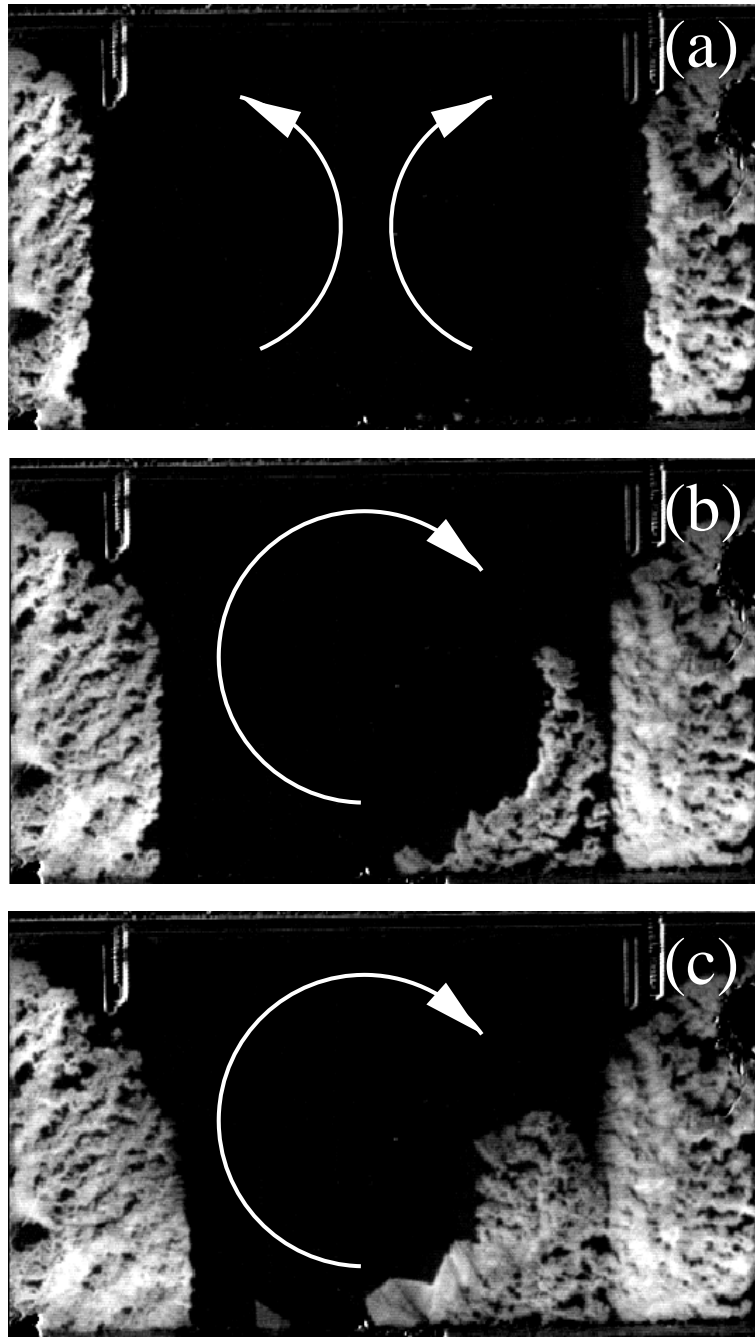


FIG. 4. Sequence of images showing aggregation phenomena when the NH_4Cl solution is heated from below in a 0.10 cm thick cell; temperatures: $T_h = 16^\circ C$, $T_o = 22^\circ C$, and $T_c = -3^\circ C$. The images show the full 8.0 cm x 16.0 cm inner cell. Times after the start of run are: (a) 9 min, (b) 18 min and (c) 26 min. Arrows have been added to indicate the convective flows in the system. The entire inner cell (8.0 cm x 16.0 cm) is visible in these images.

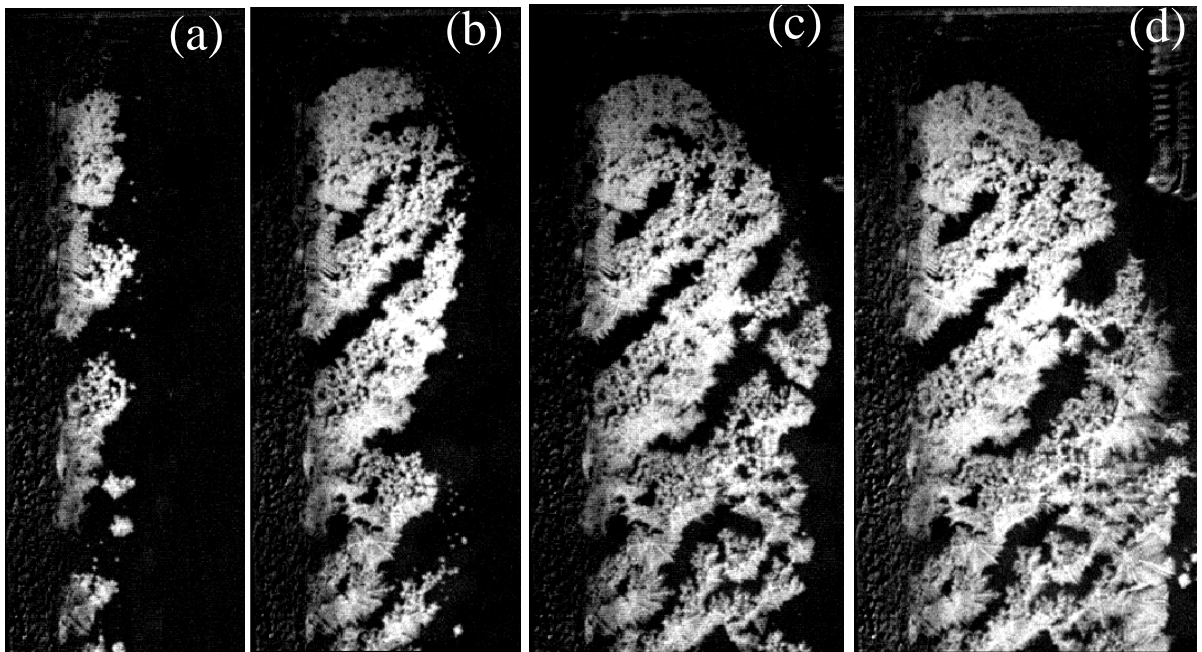


FIG. 5. Close up of the developing aggregation patterns at the left side of the cell; same conditions as for Fig. 4. Times after start of run: (a) 6 min, (b) 8.5 min, (c) 11.5 min and (d) 15.5 min. In all of these figures, the top 5.0 cm of the left side of the inner cell is shown.

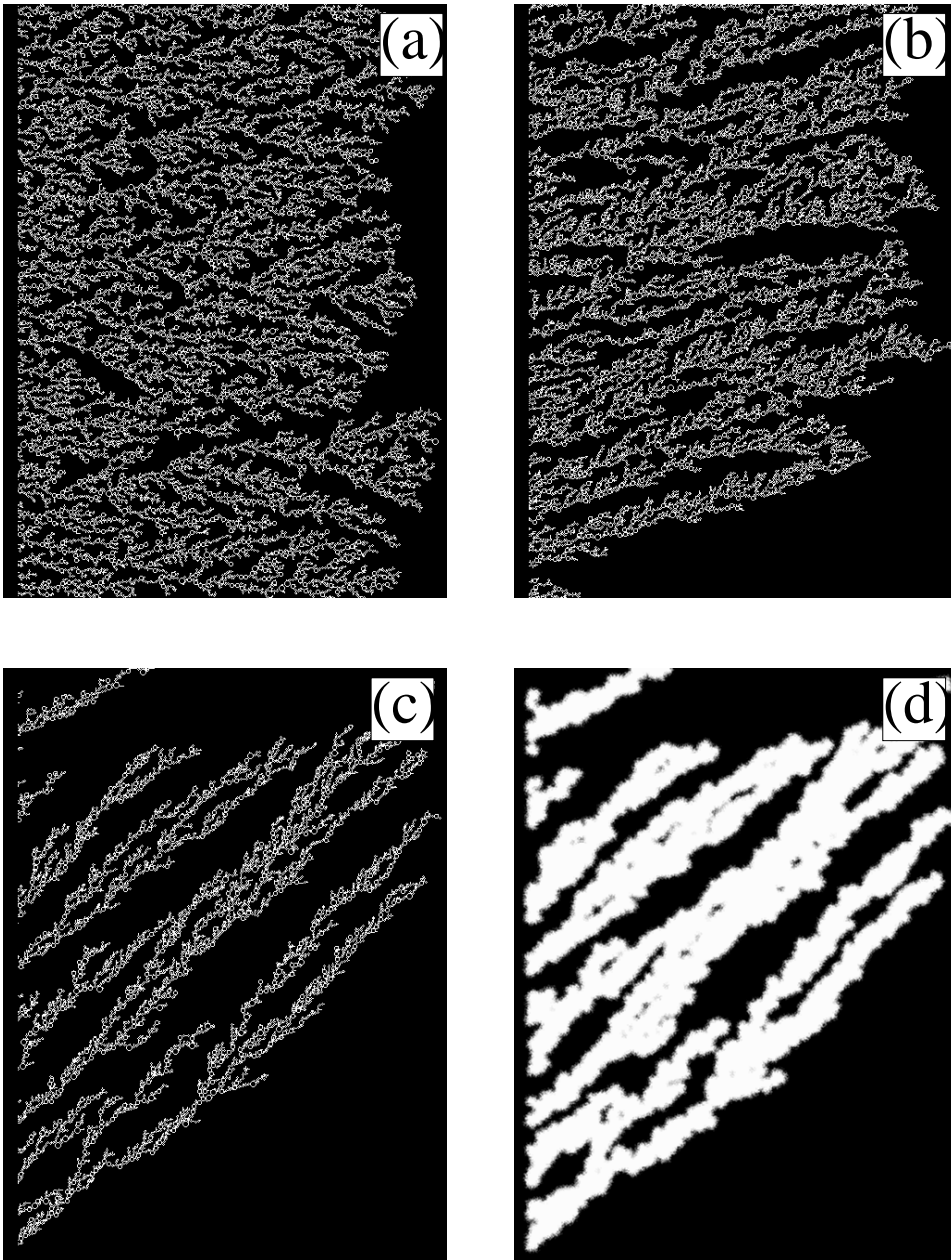


FIG. 6. Simulations of aggregation phenomena. Deposition angle α (relative to the normal to the side-wall): (a) 0 degrees; (b) 37 degrees; (c) 72 degrees; (d) 72 degrees, but with implementation of dilation to show the effects of dendritic broadening (see text).

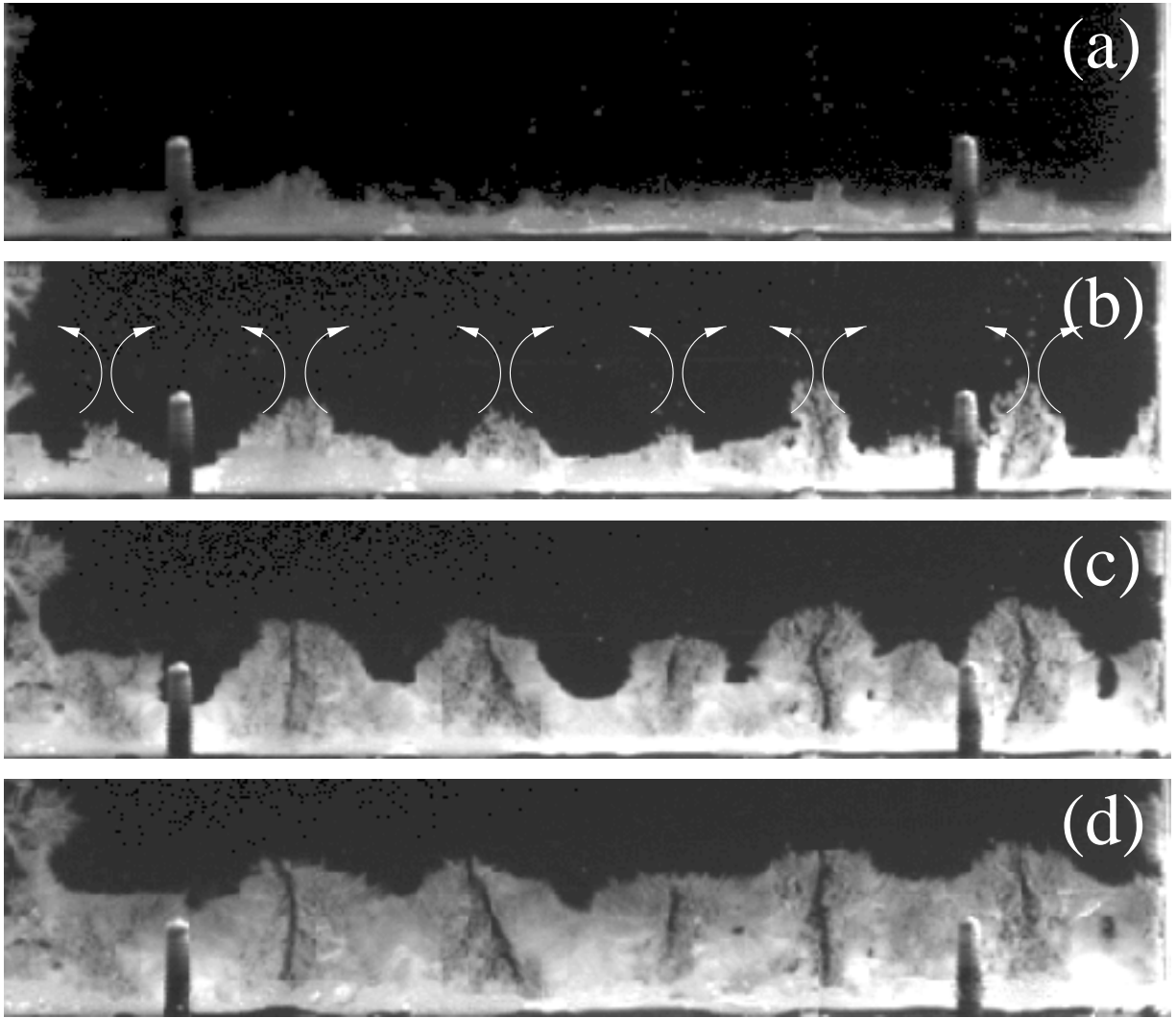


FIG. 7. Aggregation-enhanced chimney formation in cell cooled from below with a cool outer temperature T_o . Temperatures are $T_c = -10^\circ\text{C}$, $T_h = T_o = 5.5^\circ\text{C}$ initially, then T_h and T_o are increased to 10°C as NH_4Cl “snow” begins to develop. (These temperatures should all be compared to the liquidus temperature 17°C .) Times after cool-down of bottom plate: (a) 5 min, (b) 7 min, (c) 15 min, and (d) 30 min. A “snow” of NH_4Cl seed crystals can be seen toward the right of figure (b). Arrows have been added to figure (b) to indicate the convective flows. In all of the images, the entire 16.0 cm width of the inner cell is shown.

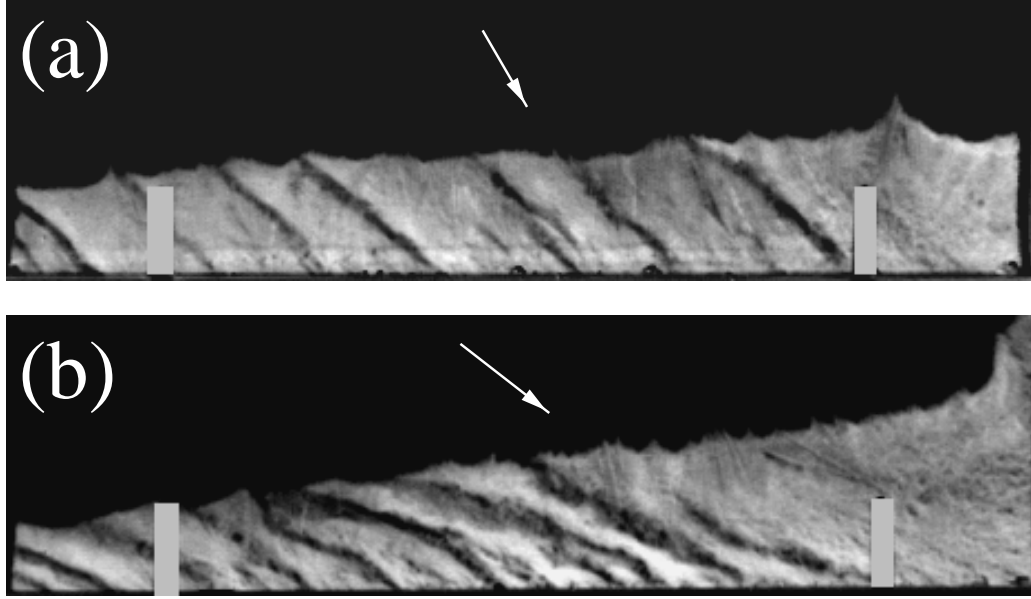


FIG. 8. Aggregation-enhanced chimney formation with the apparatus tipped; $T_h = 20.0^\circ\text{C}$, $T_o = 15.0^\circ\text{C}$, and $T_c = -10^\circ\text{C}$. In both of these images, the camera has been tipped along with the cell; the direction of gravitational acceleration is shown as arrows in these diagrams. Both images were taken 49 minutes after the start of the run. Tilt angle for cell: (a) 30° ; (b) 52° . In all of the images, the entire 16.0 cm width of the inner cell is shown.

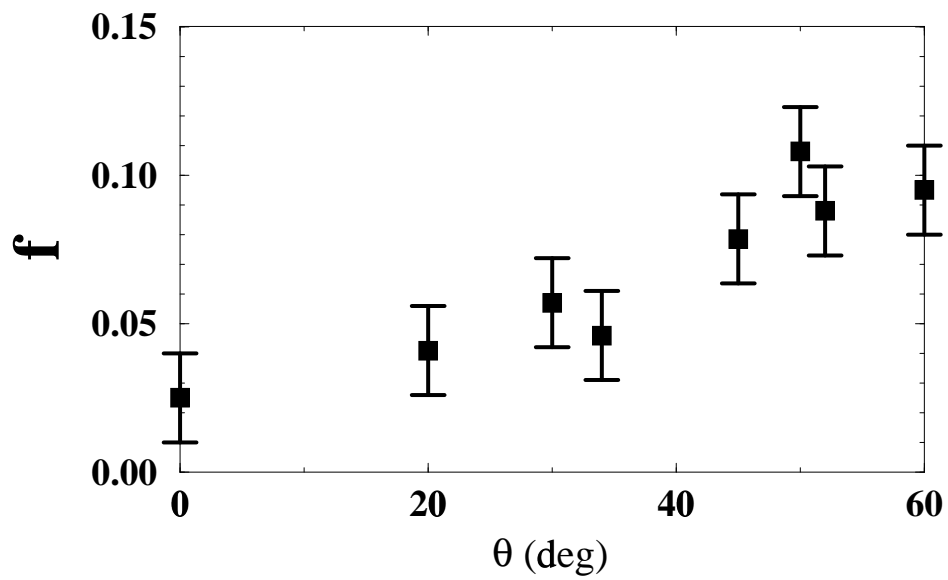


FIG. 9. Void fraction f versus tip angle θ . In all cases, the fraction was determined 50 min after start of the run.

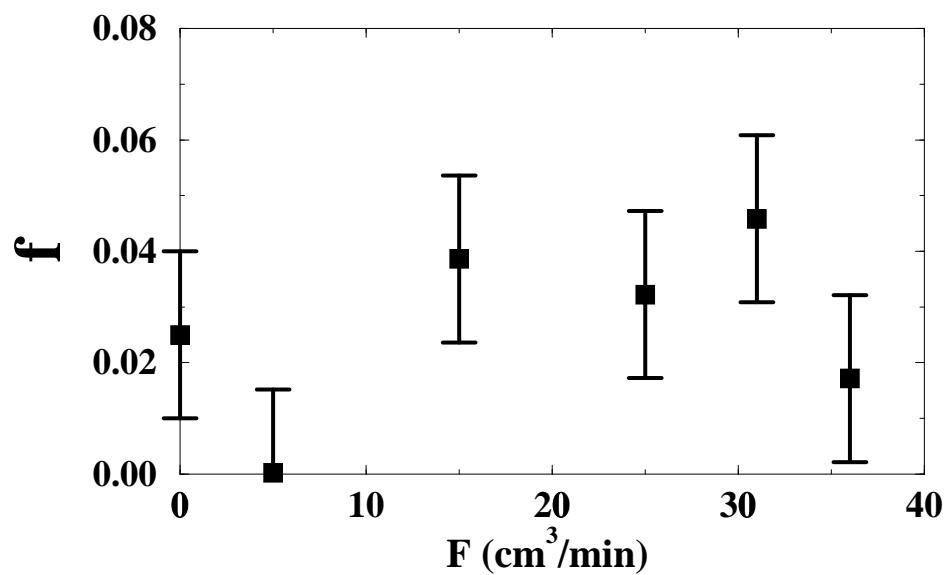


FIG. 10. Void fraction f versus shearing flow rate F ; the shearing flow is produced by peristaltic pumping. In all cases, the fraction was determined 50 min after the start of the run. For reference, the cell volume is 27 cm^3 .

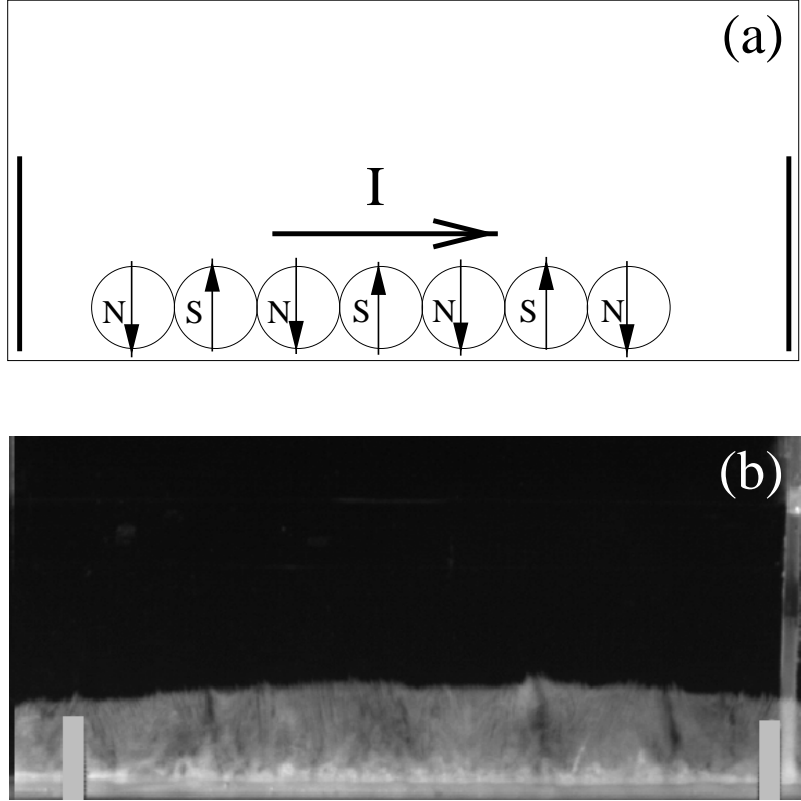


FIG. 11. Artificial forcing of fluid flows within the mushy layer. (a) Magneto hydrodynamic (MHD) forcing technique. An electrical current moving horizontally through the fluid interacts with an alternating magnetic field produced by a linear array of alternating magnets. The result is alternating up/down forcing of the fluid. (b) Experimental run; $T_h = 20.0^\circ\text{C}$, $T_c = -10^\circ\text{C}$, and $T_o = 15^\circ\text{C}$. The MHD flow was initiated 12 min after the start of the run (just as the mushy layer was growing past the region with the magnets), and the image shown was obtained 52 min after the start of the run. The middle 13 cm of the inner cell is shown in Fig. (b).

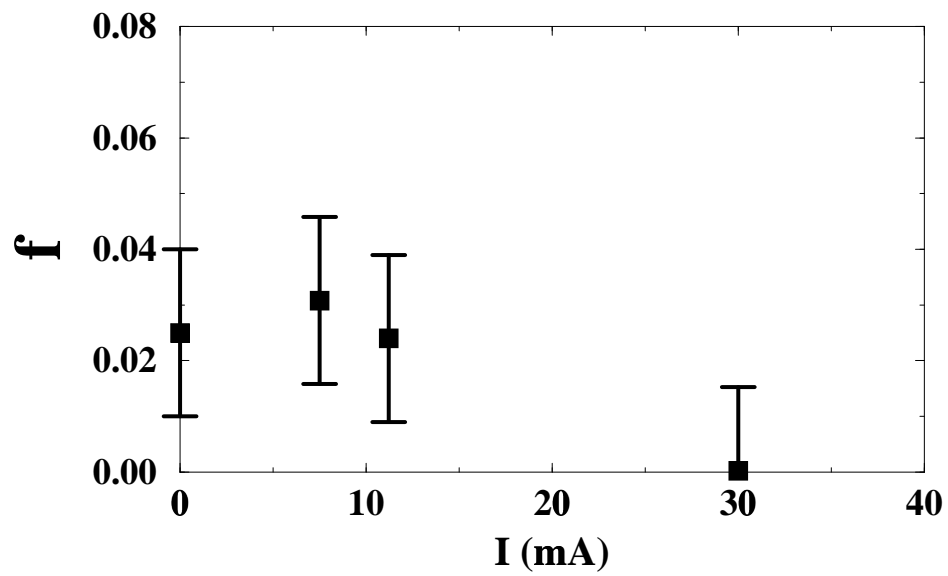


FIG. 12. Void fraction f (after 50 minutes) versus internal mushy layer forcing strength (characterized by the MHD current I).